



Consolidated method to predicting pressure drop and heat transfer coefficient for both subcooled and saturated flow boiling in micro-channel heat sinks

Sung-Min Kim, Issam Mudawar*

Boiling and Two-Phase Flow Laboratory (BTPFL), and Purdue University International Electronic Cooling Alliance (PUIECA), Mechanical Engineering Building, 585 Purdue Mall West Lafayette, IN 47907-2088, USA

ARTICLE INFO

Article history:

Received 20 December 2011
Received in revised form 13 January 2012
Accepted 17 February 2012
Available online 16 April 2012

Keywords:

Micro-channel
Subcooled boiling
Saturated boiling
Pressure drop

ABSTRACT

Published studies concerning transport phenomena in micro-channel heat sinks can be divided into those concerning saturated boiling versus those focused on subcooled boiling, with the vast majority related to the former. What has been lacking is a single generalized method to tackle both boiling regimes. The primary objective of the present paper is to construct a consolidated method to predicting transport behavior of micro-channel heat sinks incurring all possible heat transfer regimes. First, a new correlation is developed for subcooled flow boiling pressure drop that accounts for inlet subcooling, micro-channel aspect ratio, and length-to-diameter ratio. This correlation shows excellent predictive capability against subcooled HFE 7100 pressure drop data corresponding to four different micro-channel geometries. Next, a consolidated method is developed for pressure drop that is capable of tackling inlet single-phase liquid, subcooled boiling, saturated boiling, and single-phase vapor regimes as well as inlet contraction and outlet expansion. A similar consolidated method is developed to predict the heat transfer coefficient that is capable of tackling all possible combinations of heat transfer regimes. The new consolidated method is shown to be highly effective at reproducing both data and trends for HFE 7100, water and R134a.

© 2012 Elsevier Ltd. All rights reserved.

1. Introduction

The past two decades have witnessed unprecedented increases in heat dissipation in high performance computers, electrical vehicle power electronics, avionics, and directed energy laser and microwave weapon systems [1,2]. These increases spurred intense research efforts to capitalize upon the cooling merits of phase change using a variety of configurations, including spray [3–5], jet [6–9], and micro-channel cooling schemes [2,10–13], as well as techniques to enhance surface micro-structure [14].

Two-phase micro-channel heat sinks are ideally suited for modern applications demanding the dissipation of large amounts of heat within very limited space [2]. These devices are highly compact and lightweight, and require very small coolant inventory. And unlike their single-phase counterparts, which derive their performance entirely from the coolant's sensible heat rise, two-phase micro-channel heat sinks utilize both sensible and latent heat to absorb large amounts heat while maintaining relatively low surface temperatures.

The vast majority of published two-phase micro-channel studies concerns saturated boiling. With an inlet quality close to or greater than zero, small channel diameter causes any nucleation

bubbles to coalesce very quickly, resulting in mostly slug or annular flow [2]. On the other hand, subcooled boiling occurs when the coolant is supplied to the micro-channel with a thermodynamic equilibrium quality well below zero. With subcooled boiling, bubble growth is greatly suppressed, resulting in a relatively mild increase in void fraction along the channel, especially for high mass velocities. Because of the relatively short length of micro-channels in practical two-phase heat sinks, subcooled conditions may persist to the channel outlet. This greatly enhances the ability to dissipate very large heat fluxes by capitalizing upon the coolant's combined sensible and latent heat compared to mostly latent heat for saturated flow boiling. This is evident from a study by Lee and Mudawar [15,16], which yielded heat fluxes as high as 840 W/cm² with HFE 7100 without encountering critical heat flux (CHF).

Because of small void fraction in subcooled boiling, both the pressure drop and heat transfer characteristics in subcooled micro-channel flow are categorically different from those for saturated boiling. Since most studies on flow boiling in micro-channels have been focused on the saturated boiling regime, there has been significant progress in the development of predictive tools for both pressure drop and heat transfer coefficient for saturated boiling [17–22]. As indicated in [15,16], far little progress has been made in the prediction of subcooled flow boiling in micro-channels.

One objective of the present study is to further the understanding of subcooled flow boiling in micro-channel heat sinks begun by Lee and Mudawar [15,16] by providing more accurate tools for the

* Corresponding author. Tel.: +1 (765) 494 5705; fax: +1 (765) 494 0539.

E-mail address: mudawar@ecn.purdue.edu (I. Mudawar).

URL: <https://engineering.purdue.edu/BTPFL> (I. Mudawar).

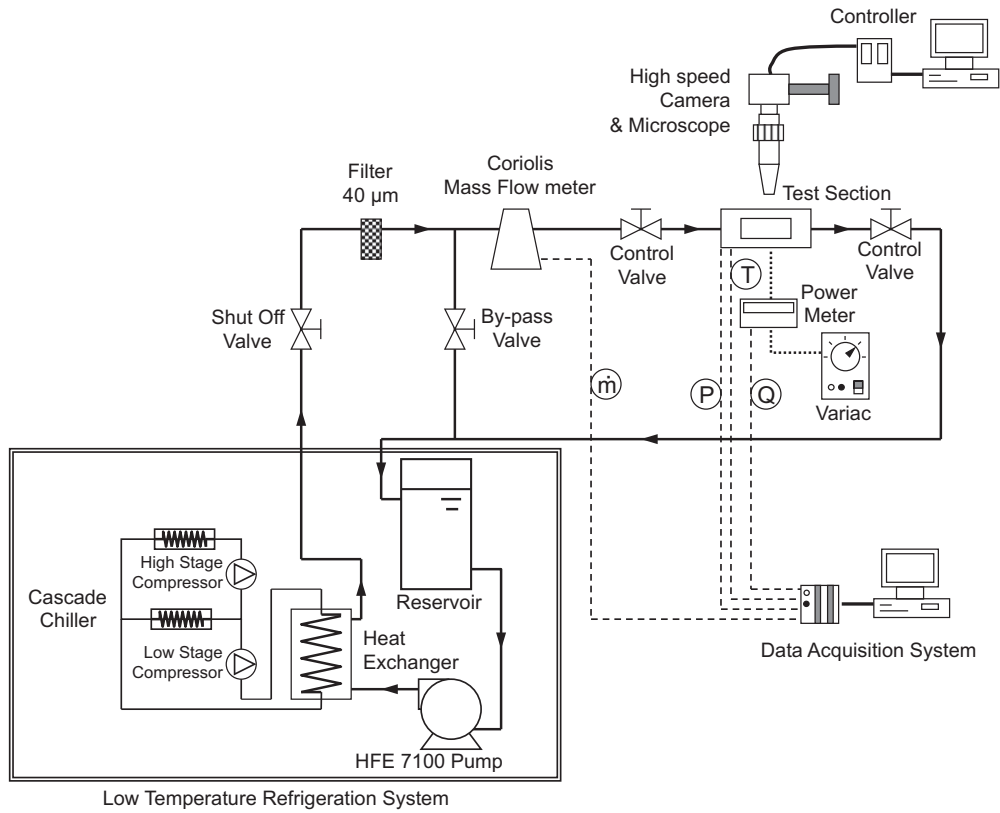


Fig. 1. Schematic diagram of coolant conditioning system.

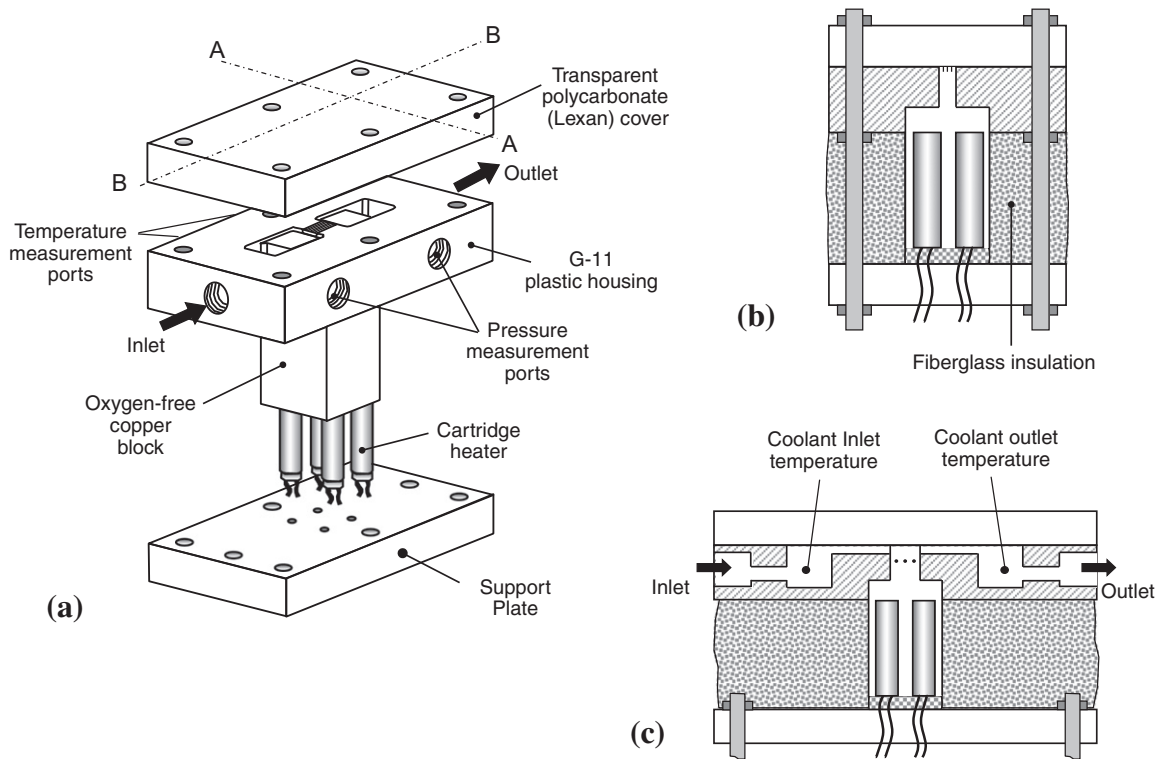


Fig. 2. (a) Isometric view of micro-channel test section. (b) Cross-sectional view (A-A). (c) Side sectional view (B-B).

used to insulate the top portion of the copper block. This housing also contains coolant inlet and outlet ports, micro-channel inlet and outlet plenums, and instrumentation ports for both pressure

and temperature measurements in both the inlet and outlet. A transparent polycarbonate plastic cover plate serves as top insulating surface for the micro-channels and facilitates optical access to

the boiling flow. The lower surfaces of the copper block are covered with fiberglass insulation to minimize heat loss to the ambient.

Four different copper blocks (TS #1 – TS #4) are used to test the influence of micro-channel size. These blocks possess identical 0.5 cm wide by 1.0 cm long top heat transfer areas but different micro-channel features. These features are detailed in Table 1 in terms of channel width, W_{ch} , channel height, H_{ch} , width of metal wall separating micro-channels, W_s , channel width-to-channel height aspect ratio, β , and number of parallel micro-channels, N . Also included in Table 1 are the operating conditions for each test section in terms of coolant inlet temperature, T_{in} , total mass flow rate, \dot{m} , outlet pressure, P_{out} , mass velocity, G , and range of heat flux, q'' .

Three type-T thermocouples are inserted in the copper block beneath the micro-channels as illustrated in Fig. 2(c). The thermocouple measurements ($T_{tc,1}, T_{tc,2}, T_{tc,3}$) are used to calculate heat transfer coefficients and wall temperatures at the base of the micro-channel ($T_{w,1}, T_{w,2}, T_{w,3}$) immediately above using a fin analysis method and the assumption of 1-D vertical conduction as discussed in Ref. [15].

Other measurements include electrical power input to the test section's four cartridge heaters using a Wattmeter, and mass flow rate using the Coriolis flow meter. All measurements are made simultaneously and processed by an HP3852 data acquisition system.

A systematic iterative numerical scheme is used to calculate heat loss from the copper block. As detailed in Ref. [15], heat loss is estimated at 14 to 20% of electrical power input for single-phase conditions, and 6 to 14% for two-phase conditions. The experimental data presented in this paper are corrected for this heat loss.

Uncertainties in the thermocouple measurements are $\pm 0.3^\circ\text{C}$, and the accuracies of the other measurement instruments are as follows: $\pm 0.5\%$ for the pressure transducers, $\pm 0.1\%$ for the Coriolis flow meter, and $\pm 0.1\%$ for the Wattmeter. Additional details concerning the system construction and operation, heat loss calculation and measurement accuracies are available in Ref. [15].

3. Determination of subcooled boiling pressure drop correlations

3.1. Assessment of prior subcooled pressure drop correlations

As indicated earlier, predictive tools for subcooled flow boiling are quite sparse, and recommended mostly for water flow in circular tubes. Table 2 provides a summary of prior subcooled boiling pressure drop correlations whose predictions are compared to the present HFE 7100 data. These correlations are presented as a ratio of subcooled boiling pressure drop to pressure drop for adiabatic flow (zero heat flux) at the same mass velocity. Most include the ratio of subcooled boiling length to saturated boiling length, L_{sc}/L_{sat} , where L_{sc} is the length from the incipient boiling location to the exit, and L_{sat} from the incipient boiling location to the location where the fluid would reach saturation state. Owens and Schrock's rather simple correlation [23], which is a function of L_{sc}/L_{sat} alone, was developed for water flow in tubes with diameters of 3

and 4.6 mm. The correlation of Tarasova et al. [24], which accounts for both boiling number and ratio of liquid-to-vapor specific volume, covers a broad range of pressures (9.8 to 196 bar) for water flow in tubes with diameters of 2.89, 6.34, and 8.31 mm. Hahne et al.'s correlations [25] were derived from data for water and refrigerants R12 and R134a, and are applicable for both tubes and annuli with hydraulic diameters from 9.53 to 20 mm. Aside from the parameters in Tarasova et al.'s correlation, the correlations by Hahne et al. also account for the effects of modified Jakob number, and ratio of the flow channel's heated to wetted perimeters. The correlations of Tong et al. [26], which are based on L_{sc}/L_{sat} alone, are recommended for water flow in tubes with diameters of 1.05–2.44 mm and two different length-to-diameter ratios.

Fig. 3(a)–(c) compare the predictions of the correlations by Owens and Schrock [23] and Hahne et al. [25] (for water), and Tong et al. [26]'s correlations, respectively, to the present HFE 7100 experimental data. The predictive accuracy of the correlations is measured by mean absolute error, which is defined as

$$MAE = \frac{1}{M} \sum \left[\frac{\Delta P_{sc}/\Delta P_{ad,pred} - \Delta P_{sc}/\Delta P_{ad,exp}}{\Delta P_{sc}/\Delta P_{ad,exp}} \right] \times 100 \quad (1)$$

Fig. 3(a)–(c) show the present data are overpredicted by all three correlations, with MAEs of 90.1%, 140.3% and 97.7%, for Owens and Schrock, Hahne et al. and Tong et al., respectively. In Fig. 3(c), the Tong et al. correlation corresponding to $L/D_h = 50$ is used for TS #1 and TS #2, and the correlation corresponding to $L/D_h = 25$ for TS #3 and TS #4. Overall, the correlation for $L/D_h = 50$ gives superior predictions for TS #1 and TS #2 compared $L/D_h = 25$ for TS #3 and TS #4. Similarly, Hahne et al.'s correlation shows better predictions for TS #1 and TS #2 compared to TS #3 and TS #4. The predictions of Tarasova et al. [24] are not shown in Fig. 3 because of the unusually large MAE (1227%) for this specific correlation.

Overall, the lack of predictive accuracy depicted in Fig. 3(a)–(c) can be attributed to differences in working fluid, hydraulic diameter, mass velocity, and pressure between the present data and the data these correlations are based upon.

3.2. New subcooled pressure drop correlation

A new correlation is therefore sought that can more accurately determine subcooled pressure drop for dielectric fluids and rectangular micro-channels recommended for cooling high-flux electronic and power devices. This is achieved by correlating a subset of the present HFE 7100 database corresponding to conditions where subcooled boiling is observed over the entire length, i.e., $L_{sc} = L$.

For a rectangular micro-channel with negligible reduction in saturation pressure in the single-phase region, L_{sat} can be expressed as

$$L_{sat} = \frac{GW_{ch}H_{ch}}{q''(W_{ch} + W_s)} c_{pf}(T_{sat} - T_f)_{in} \quad (2)$$

Fig. 4(a) shows the influence of inlet subcooling ($T_{in} = 0$ and -30°C) on subcooled boiling pressure drop for TS #3 with $\dot{m} = 2\text{--}5$ g/s.

Table 1
Micro-channel dimensions and operating conditions for four test sections.

	W_{ch} μm	H_{ch} μm	W_s μm	β –	D_h μm	L cm	N –	T_{in} $^\circ\text{C}$	\dot{m} g/s	P_{out} bar	G kg/m ² s	q'' W/cm ²
TS #1	123.4	304.9	84.2	0.40	175.7	1.0	24	–30, 0	2.0–5.0	1.138	2200–5550	0–560
TS #2	123.4	526.9	84.6	0.23	200.0	1.0	24	–30, 0	2.0–5.0	1.138	1280–3210	0–580
TS #3	235.2	576.8	230.3	0.41	334.1	1.0	11	–30, 0	2.0–5.0	1.138	1330–3350	0–640
TS #4	259.9	1041.3	205.0	0.25	415.9	1.0	11	–30, 0	2.0–5.0	1.138	670–1683	0–664

Table 2
Prior subcooled boiling pressure drop correlations and their MAE in predicting present HFE 7100 data.

Authors	Correlations	Remarks	MAE
Owens and Schrock [23]	$\frac{\Delta P_{sc}}{\Delta P_{ad}} = 0.97 + 0.028 \exp\left(6.13 \frac{L_{sc}}{L_{sat}}\right)$	Water $D = 3.4, 6.3 \text{ mm}$ $q''_{ch} = 67.5\text{--}400.6 \text{ W/cm}^2$ $G = 1143\text{--}5322 \text{ kg/m}^2\text{s}$ $P = 3.4\text{--}27.6 \text{ bar}$	90.1%
Tarasova et al. [24]	$\frac{\Delta P_{sc}}{\Delta P_{ad}} = 1 + Bo^{0.7} \left(\frac{v_{ch}}{v_f}\right)^{0.78} \frac{20L_{sc}/L_{sat}}{1.315 - L_{sc}/L_{sat}}$ where $Bo = q''_{ch}/Gh_{fg}$	Water $D = 2.89, 6.34, 8.31 \text{ mm}$ $q''_{ch} = 58\text{--}175 \text{ W/cm}^2$ $G = 1400\text{--}3000 \text{ kg/m}^2\text{s}$ $P = 9.8\text{--}196 \text{ bar}$	1227%
Hahne et al. [25]	$\frac{\Delta P_{sc}}{\Delta P_{ad}} = 1 + CBo^{1.6}Ja^{*-1.2} \frac{v_{ch}}{v_f} \frac{P_H}{P_F}$ $C = 80$ for water and 500 for R12 and R134 where $Ja^* = c_{p,f} \Delta T_{sub,in}/h_{fg}$	Water, R12, R134a $D_h = 9.53\text{--}20 \text{ mm}$ $q''_{ch} = 0.52\text{--}96 \text{ W/cm}^2$ $G = 750\text{--}3200 \text{ kg/m}^2\text{s}$ $P = 3\text{--}20 \text{ bar}$	140% for $C = 80$ 955% For $C = 500$
Tong et al. [26]	$\frac{\Delta P_{sc}}{\Delta P_{ad}} = \left(\frac{L_{sc}}{L_{sat}}\right)^{1.3} \exp\left(\frac{L_{sc}}{L_{sat}} + 0.4\right)$, for $\frac{L}{D_h} = 50$ $\frac{\Delta P_{sc}}{\Delta P_{ad}} = \left(\frac{L_{sc}}{L_{sat}}\right)^{1.3} \exp\left(\frac{L_{sc}}{L_{sat}} + 1.35\right)$, for $\frac{L}{D_h} = 25$	Water $D = 1.05\text{--}2.44 \text{ mm}$ $q''_{ch,CHF} = 5000\text{--}8000 \text{ W/cm}^2$ $G = 25000\text{--}45000 \text{ kg/m}^2\text{s}$ $P_{out} = 4\text{--}16 \text{ bar}$	97.7%

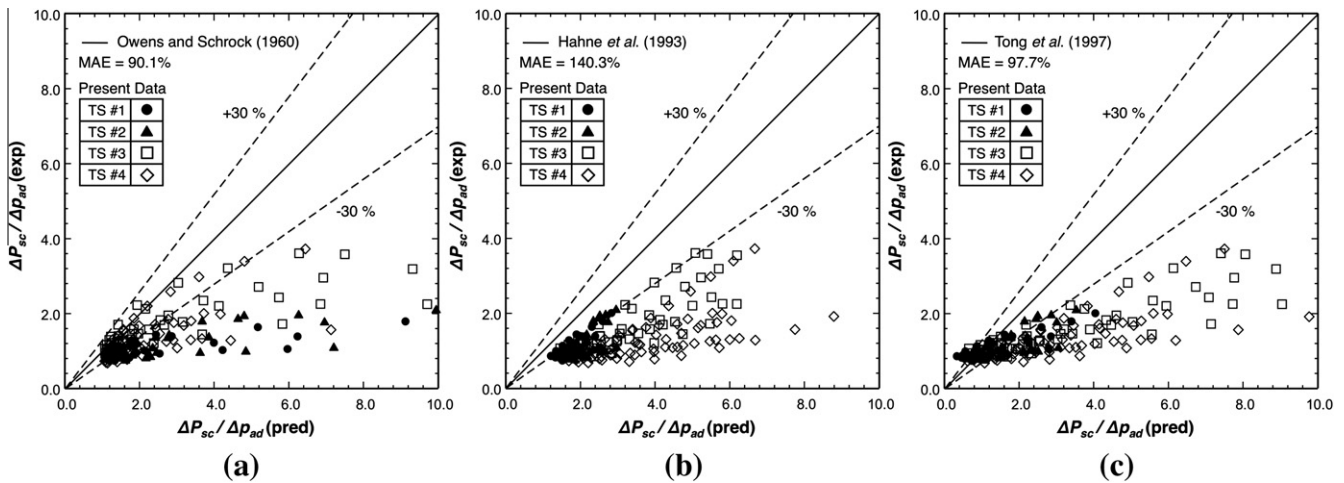


Fig. 3. Comparison of predictions of subcooled pressure drop correlations of (a) Owens and Schrock [23], (b) Hahne et al. [25], and (c) Tong et al. [26] with present HFE 7100 data for four micro-channel test sections.

Experimental data are clustered into two different groups that display nearly constant slope that increases with decreasing inlet subcooling. Using the entire subcooled database for all four test sections, the ratio of subcooled boiling pressure drop to adiabatic pressure drop is correlated as a linear function of the length ratio L_{sc}/L_{sat} .

$$\frac{\Delta P_{sc}}{\Delta P_{ad}} = 20.73 Ja^{*-0.98} \beta^{0.42} \left(\frac{L}{D_h}\right)^{-0.54} \frac{L_{sc}}{L_{sat}}, \quad (3)$$

where

$$Ja^* = \frac{c_{p,f} \Delta T_{sub,in}}{h_{fg}} \quad (4)$$

and

$$\beta = \frac{W_{ch}}{H_{ch}}. \quad (5)$$

Fig. 4(a) shows Eq. (3) provides good agreement with the data for both inlet temperatures. Fig. 4(b) shows the new correlation

predicts the subcooled data for all four micro-channel test sections with a mean absolute error of 15.3%, with most of the data falling within $\pm 30\%$ of predicted values.

4. Predictive method for micro-channel heat sink pressure drop

A complete methodology for predicting pressure drop in two-phase micro-channel heat sinks must be able to tackle both subcooled and saturated flow conditions and account for inlet contraction pressure drop, inlet single-phase liquid region, and outlet recovery. The total pressure drop, ΔP_{tot} , can therefore be the sum of the contributions of inlet contraction (single-phase liquid or saturated mixture), ΔP_c , upstream single-phase liquid region, ΔP_{sp} , subcooled two-phase region, ΔP_{sc} , saturated two-phase region (friction and acceleration), ΔP_{sb} , and outlet expansion recovery (saturated mixture), ΔP_e .

$$\Delta P_{tot} = \Delta P_c + \Delta P_{sp,u} + (\Delta P_{sc} + \Delta P_{sb}) + \Delta P_{sp,d} + \Delta P_e. \quad (6)$$

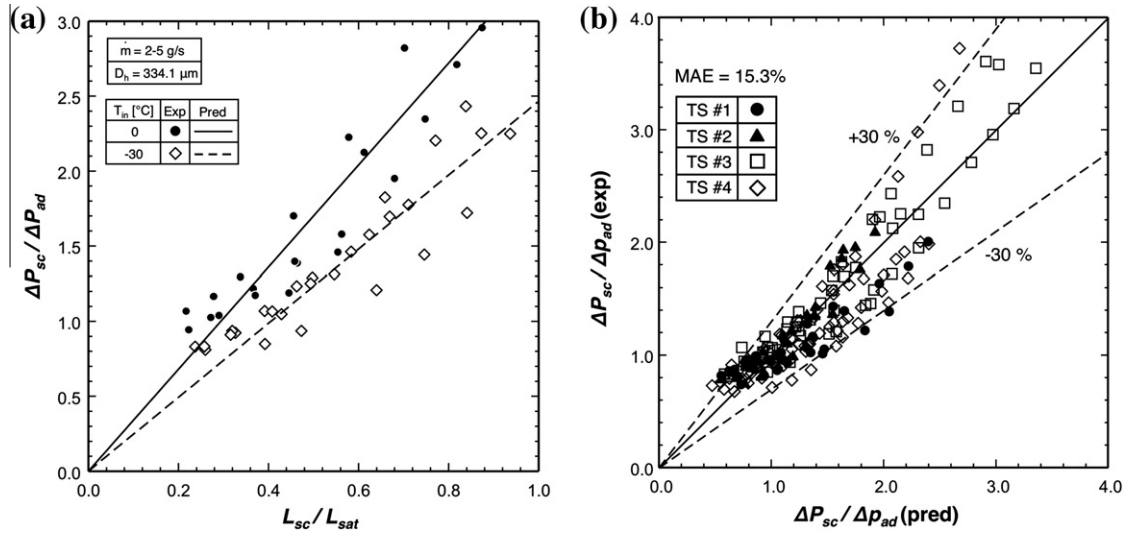


Fig. 4. Variation of ratio of HFE 7100 subcooled pressure drop to adiabatic pressure drop with ratio of subcooled to saturated length for TS #3 for two inlet temperatures. (b) Comparison of predictions of new subcooled pressure drop correlation and experimental HFE 7100 data for four micro-channel test sections.

4.1. Inlet contraction

The contraction pressure loss at the micro-channel inlet is determined from relations by Collier and Thome [27],

$$\Delta P_c = \frac{G^2 v_f}{2} \left[\left(\frac{1}{C_c} - 1 \right) + (1 - \sigma_c^2) \right] \left[1 + \frac{v_{fg} x_{e,in}}{v_f} \right], \quad (7)$$

where

$$\sigma_c = \frac{W_{ch} H_{ch} N}{W_p H_p}, \quad (8)$$

For single-phase flow at the plenum inlet, the contraction coefficient, C_c , in Eq. (7) associated with vena-contracta is obtained from a relation by Geiger [28],

$$C_c = 1 - \frac{1 - \sigma_c}{2.08(1 - \sigma_c) + 0.5371}. \quad (9)$$

For two-phase flow at the inlet, the effect of vena-contracta is neglected based on recommendations by Schmidt and Friedel [29] and Abdelal et al. [30], and $C_c = 1$.

4.2. Upstream single-phase liquid region

Pressure drop for the upstream single-phase liquid region is given by

$$\Delta P_{sp,u} = \frac{2f_{app} G^2 L_{sp,u} v_f}{D_h}. \quad (10)$$

The apparent single-phase friction factor, f_{app} , in Eq. (10) is determined according to an empirical formula of a Churchill and Usagi type [31] obtained by Copeland [32] using data from Shah and London [33].

$$f_{app} Re_{sp,u} = \left\{ \left[3.2 \left(\frac{L_{sp,u}}{Re_{sp,u} D_h} \right)^{-0.57} \right]^2 + (f_{sp,u} Re_{sp,u})^2 \right\}^{1/2}, \quad (11)$$

where

$$f_{sp,u} Re_{sp,u} = 24(1 - 1.3553\beta + 1.9467\beta^2 - 1.7012\beta^3 + 0.9564\beta^4 - 0.2537\beta^5). \quad (12)$$

For the turbulent developing liquid flow region, the local pressure is predicted according to Zhi-qing's analytical solution for a circular

tube [34] based on the axial extent of the turbulent single-phase region,

$$L_{sp,u}/D_h = 1.4039 Re_{sp,u}^{0.25} \delta^{+1.25} (1 + 0.1577\delta^+ - 0.1793\delta^{+2} - 0.0168\delta^{+3} + 0.0064\delta^{+4}). \quad (13)$$

where δ^+ is the dimensionless thickness of the hydrodynamic boundary layer. For the turbulent developing region ($\delta^+ < 1$),

$$f_{app} = \left[\frac{1}{(1 - 0.25\delta^+ + 0.0667\delta^{+2})^2} - 1 \right] \frac{0.25}{L_{sp,u}/D_h}. \quad (14)$$

For the turbulent fully-developed region, $\delta^+ = 1$, which reduced Eq. (13) to

$$L_{sp,u}/D_h = 1.3590 Re_{sp,u}^{0.25}, \quad (15)$$

and Eq. (14) to

$$f_{app} = \left(0.07 + 0.316 \frac{L_{sp,u}/D_h}{Re_{sp,u}^{0.25}} \right) \frac{0.25}{L_{sp,u}/D_h} \quad (16)$$

4.3. Subcooled two-phase region

The upstream edge of the two-phase region corresponds to the onset of nucleate boiling, which is predicted according to Sato and Matsumura's relation [35]

$$q''_{ch,ONB} = \frac{k_f h_{fg} \rho_g (T_w - T_{sat})^2}{8\sigma T_{sat}}. \quad (17)$$

Pressure drop in the subcooled two-phase region is predicted according to Eq. (3) derived in the previous section.

4.4. Saturated two-phase region

Pressure drop in the saturated two-phase region is composed of frictional and accelerational components.

$$\Delta P_{sb} = \Delta P_{sb,F} + \Delta P_{sb,A}. \quad (18)$$

The frictional pressure drop is evaluated by both the Lee and Mudawar [21] correlation for laminar liquid-laminar vapor (vv) and laminar liquid-turbulent vapor (vt) flow regimes, and the Lee

and Lee [13] correlation for turbulent liquid-turbulent vapor (tt) flow regime. Notice that the Lee and Mudawar correlation accounts for the effects of liquid viscosity and surface tension on the two-phase pressure drop multiplier based on the separated flow model.

$$\Delta P_{sb,F} = \frac{2G^2 L_{sb}}{D_h x_{e,out}} \int_0^{x_{e,out}} f_f (1 - x_e)^2 v_f \phi_f^2 dx_e. \quad (19)$$

The two-phase multiplier in the above equation is given by

$$\phi_f^2 = 1 + \frac{C}{X} + \frac{1}{X^2}, \quad (20)$$

where

$$X^2 = \frac{(dP/dz)_f}{(dP/dz)_g}, \quad (21)$$

$$C = C_{lv} = 2.16 \text{Re}_{fo}^{0.047} \text{We}_{fo}^{0.60} \quad (\text{laminar liquid-laminar vapor}), \quad (22a)$$

$$C = C_{vt} = 1.45 \text{Re}_{fo}^{0.25} \text{We}_{fo}^{0.23} \quad (\text{laminar liquid-turbulent vapor}), \quad (22b)$$

$$C = C_{tt} = 0.048 \text{Re}_{fo}^{0.451} \quad (\text{turbulent liquid-turbulent vapor}), \quad (22c)$$

$$\text{Re}_{fo} = \frac{GD_h}{\mu_f} \quad (23)$$

and

$$\text{We}_{fo} = \frac{G^2 D_h}{\sigma \rho_f} \quad (24)$$

The accelerational component is evaluated according to [21],

$$P_{sb,A} = G^2 \left\{ \left[\frac{v_g x_{e,out}^2}{\alpha_{out}} + \frac{v_f (1 - x_{e,out})^2}{(1 - \alpha_{out})} \right] - \left[\frac{v_g x_{e,in}^2}{\alpha_{in}} + \frac{v_f (1 - x_{e,in})^2}{(1 - \alpha_{in})} \right] \right\} \quad (25)$$

using Zivi's [36] void fraction correlation,

$$\alpha = \left[1 + \left(\frac{1 - x_e}{x_e} \right) \left(\frac{v_f}{v_g} \right)^{2/3} \right]^{-1}. \quad (26)$$

4.5. Downstream single-phase vapor region

When the two-phase fluid evaporates to pure vapor in the downstream region of the micro-channel, the pressure drop for the single-phase vapor region, where the flow is assumed fully-developed, can be determined from [33,37]

$$\Delta P_{sp,d} = \frac{2f_{sp,d} G^2 L_{sp,d} v_f}{D_h} \quad (27)$$

where

$$f_{sp,d} \text{Re}_{sp,d} = 24(1 - 1.3553\beta + 1.9467\beta^2 - 1.7012\beta^3 + 0.9564\beta^4 - 0.2537\beta^5) \quad (28a)$$

$$\text{for } \text{Re}_{sp,d} < 2,000, \quad (28a)$$

$$f_{sp,d} = 0.079 \text{Re}_{sp,d}^{-0.25} \quad \text{for } 2000 \leq \text{Re}_{sp,d} < 20,000, \quad (28b)$$

and

$$f_{sp,d} = 0.046 \text{Re}_{sp,d}^{-0.2} \quad \text{for } \text{Re}_{sp,d} \geq 20,000. \quad (28c)$$

4.6. Downstream expansion pressure recovery

The expansion recovery at the micro-channel outlet is determined from a relation by Collier and Thome [27].

$$\Delta P_e = G^2 \sigma_e (\sigma_e - 1) v_f \left[1 + \frac{v_{fg} x_{e,out}}{v_f} \right] \quad (29)$$

where

$$\sigma_e = \frac{W_{ch} H_{ch} N}{W_p H_p} \quad (30)$$

5. Predictive method for micro-channel heat sink heat transfer

A complete method for predicting the heat transfer coefficient for micro-channel heat sinks must account for the upstream single-phase liquid region, subcooled boiling region and saturated boiling region.

5.1. Upstream single-phase liquid region

The local Nusselt number for the thermally developing laminar region is determined according to the following relation by Cope-land [32] obtained by fitting data from Shah and London [33].

$$\text{Nu}_x = \left\{ \left[1.54 \left(\frac{L_{sp}}{\text{Re}_{sp} \text{Pr}_f D_h} \right)^{-0.33} \right]^4 + \text{Nu}_3^4 \right\}^{1/4} \quad (31)$$

where

$$\text{Nu}_3 = 8.235(1 - 1.833\beta + 3.767\beta^2 - 5.814\beta^3 + 5.361\beta^4 - 2.0\beta^5). \quad (32)$$

The local Nusselt number for the thermally developing turbulent liquid region with constant wall heat flux is determined from the following relation by Al-Arabi [38],

$$\text{Nu}_x = \text{Nu}_{turb} \left[1 + \frac{(L_{sp}/D_h)^{-0.9}}{10 \text{Pr}_f^{1/6}} \left(0.68 + \frac{3000}{\text{Re}_{sp}^{0.81}} \right) \right] \quad (33)$$

where

$$\text{Nu}_{turb} = 0.023 \text{Re}_{sp}^{0.8} \text{Pr}_f^4. \quad (34)$$

Notice that Eq. (34) is the Dittus-Boetler equation for turbulent fully developed flow.

It should be noted that the equations of Zhi-qing [34] and Al-Arabi [38] for the turbulent developing region were developed for circular tubes, therefore the hydraulic diameter, D_h , is used instead of the tube diameter in the original equations.

5.2. Subcooled two-phase region

The variation of wall temperature in the subcooled boiling region is determined from the normalized heat transfer correlation of Lee and Mudawar [16].

$$\frac{\text{Nu}_{sc}}{\text{Nu}_{sp}} = 90.0 \text{Bo}^{+0.9} \text{Ja}^{*-0.98} \text{We}^{*0.15} \beta^{0.42} \quad (35)$$

where

$$\text{Bo}^* = \frac{q''}{G h_{fg}} \quad (36)$$

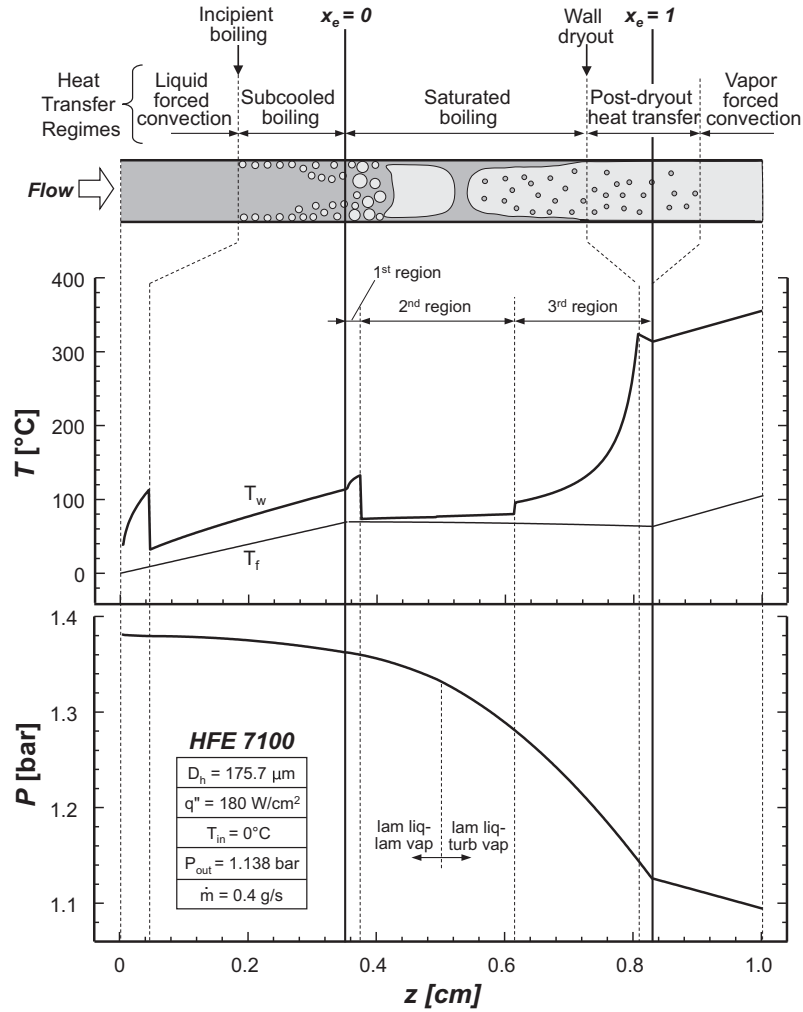


Fig. 5. Schematic of heat transfer regimes and temperature and pressure variations along micro-channel predicted using new methodology.

and

$$We^* = \frac{G^2 D_h}{(\rho_f - \rho_g) \sigma} \quad (37)$$

5.3. Saturated two-phase region

The local saturated boiling heat transfer coefficient is determined by the correlation of Lee and Mudawar [22], which consists of three different quality regions,

$$0 \leq x_e < 0.05 : h_{sb} = 3.856X^{0.267} h_{sp,f} \quad (38a)$$

$$0.05 \leq x_e < 0.55 : h_{sb} = 436.48 Bo^{0.522} We_{fo}^{0.351} X^{0.665} h_{sp,f} \quad (38b)$$

and

$$0.55 \leq x_e \leq 1.0 : h_{sb} = \max\{(108.6X^{1.665} h_{sp,g}), h_{sp,g}\} \quad (38c)$$

where

$$h_{sp,g} = \frac{Nu_3 k_g}{D_h} \quad \text{for laminar gas flow,} \quad (39)$$

$$h_{sp,g} = 0.023 Re_g^{0.8} Pr_g^{0.4} k_g / D_h \quad \text{for turbulent gas flow,} \quad (40)$$

$$Bo = \frac{q''_{ch}}{G h_{fg}}, \quad (41)$$

$$Re_g = \frac{G x_e D_h}{\mu_g} \quad (42)$$

The local saturation temperature of the fluid in the above equations is obtained from the calculated local saturation pressure, and the thermophysical properties of liquid and vapor are based on local saturation pressure.

5.4. Downstream single-phase vapor region

For the downstream single-phase vapor region, where the flow is assumed fully-developed, the local heat transfer coefficient can be determined from Eqs. (39) and (40) for laminar and turbulent gas flows, respectively.

5.5. Heat diffusion effects and onset of boiling

Determining the axial location corresponding to transition between the upstream single-phase liquid region and subcooled boiling region is based on the onset of nucleate boiling, which is influenced by heat diffusion effects in the micro-channel's cross section.

For a rectangular micro-channel heat sink with three-sided heating (i.e., with a perfectly insulating top cover plate), the local wall temperature corresponding to the bottom plane of micro-channels can be determined using the fin analysis method.

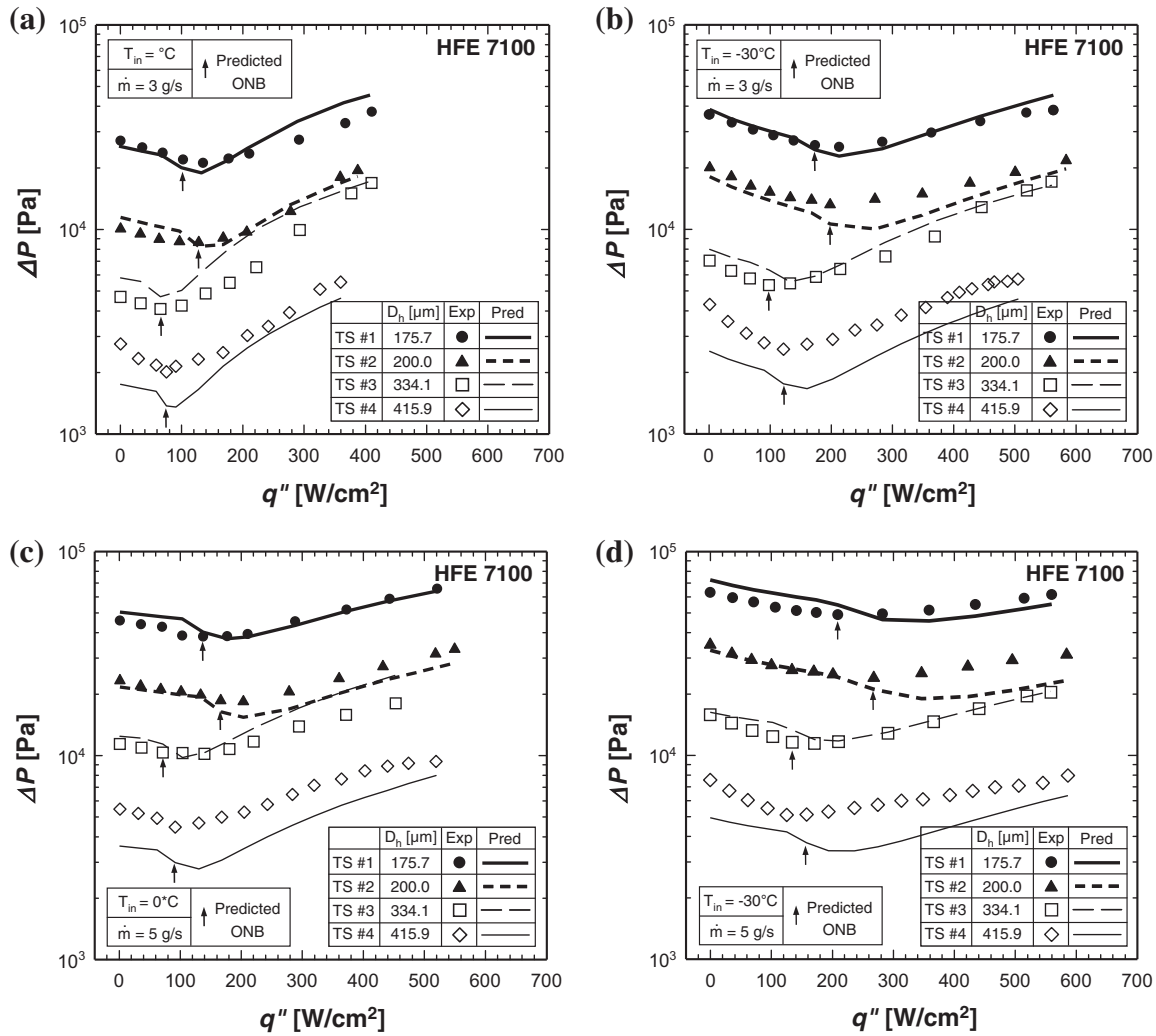


Fig. 6. Comparison of predictions of pressure drop and experimental HFE 7100 data [16] for (a) $T_{in} = 0^\circ\text{C}$ and $\dot{m} = 3 \text{ g/s}$, (b) $T_{in} = -30^\circ\text{C}$ and $\dot{m} = 3 \text{ g/s}$, (c) $T_{in} = 0^\circ\text{C}$ and $\dot{m} = 5 \text{ g/s}$, and (d) $T_{in} = -30^\circ\text{C}$ and $\dot{m} = 5 \text{ g/s}$.

$$T_w = \frac{q''(W_{ch} + W_s)}{h(W_{ch} + 2\eta H_{ch})} + T_f = \frac{q''_{ch}(W_{ch} + 2H_{ch})}{h(W_{ch} + 2\eta H_{ch})} + T_f \quad (43)$$

where the fin efficiency and fin parameter are defined, respectively, as [37]

$$\eta = \frac{\tanh(mH_{ch})}{mH_{ch}} \quad (44)$$

and

$$m = \sqrt{\frac{2h}{kW_s}} \quad (45)$$

Combining Eqs. (43) and (17), the wall temperature corresponding to the onset of boiling in a rectangular channel with three-sided heating walls can be calculated directly using

$$T_{w,ONB} = T_{sat} + \frac{4\sigma T_{sat} h(W_{ch} + 2\eta H_{ch})}{k_f h_{fg} \rho_g (W_{ch} + 2H_{ch})} \left[1 + \sqrt{1 + \frac{k_f h_{fg} \rho_g (W_{ch} + 2H_{ch})}{2\sigma T_{sat} h(W_{ch} + 2\eta H_{ch})} (T_{sat} - T_f)} \right] \quad (46)$$

Detailed analytical solutions for heat diffusion in micro-channel heat sinks having rectangular, inverse trapezoidal, triangular, trapezoidal, and diamond-shaped cross-sections for both monolithic heat sinks and heat sinks with perfectly insulating cover plates

were recently derived by the authors of the present study [39]. The authors also derived analytical power series solutions for heat diffusion in circular micro-channels with both one-sided and symmetrical two-sided heating [40].

6. Predictions and comparisons with experimental results

6.1. Overall predictive capability

Fig. 5 illustrates the overall predictive capability of the new methodology. Shown are predicted variations of wall and fluid temperatures, and pressure along the micro-channel for one of four micro-channel test sections, TS #1. The case examined here is for a constant base heat flux of $q'' = 180 \text{ W/cm}^2$ and inlet subcooling of $\Delta T_{sub,in} = 70.3^\circ\text{C}$. To avoid possible flashing phenomenon, a relatively small mass velocity of $G = 443 \text{ kg/m}^2 \text{ s}$ is examined. Notice that the new methodology is capable of identifying the axial location of the onset of nucleate boiling (ONB), and the locations where $x_e = 0$ and $x_e = 1$, thus identifying the spans of the single-phase liquid region, subcooled boiling region, saturated boiling region, and single-phase vapor region. The new methodology is capable of predicting the variations of both wall and fluid temperatures and pressure within the single-phase liquid region due to laminar/turbulent or developing/fully-developed flow effects. It is also capable of predicting the variations of wall and fluid temperatures

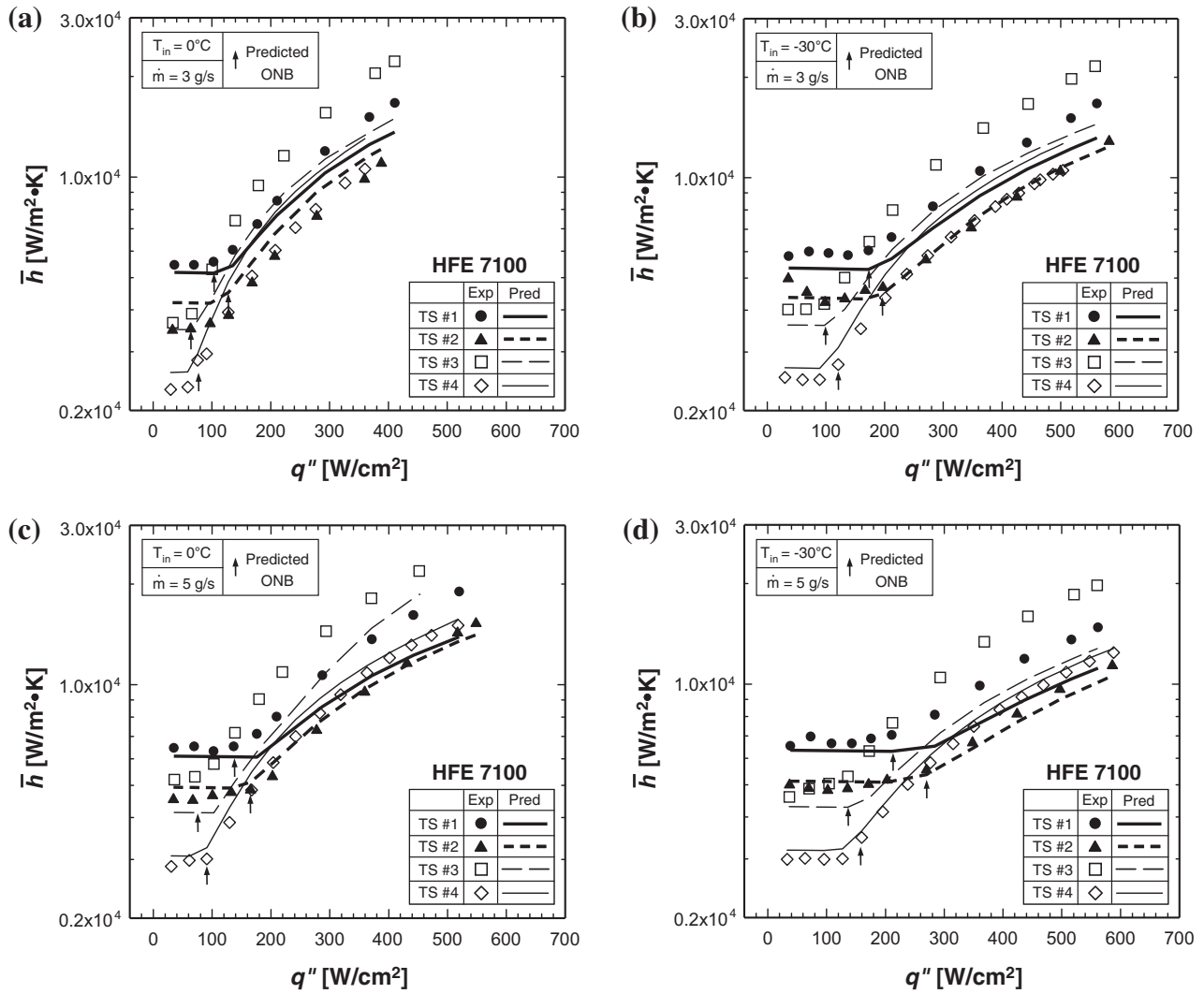


Fig. 7. Comparison of predictions of average heat transfer coefficient and experimental HFE 7100 data [16] for (a) $T_{in} = 0^\circ\text{C}$ and $\dot{m} = 3 \text{ g/s}$, (b) $T_{in} = -30^\circ\text{C}$ and $\dot{m} = 3 \text{ g/s}$, (c) $T_{in} = 0^\circ\text{C}$ and $\dot{m} = 5 \text{ g/s}$, and (d) $T_{in} = -30^\circ\text{C}$ and $\dot{m} = 5 \text{ g/s}$.

and pressure within the subcooled and saturated boiling regions separately. The wall temperature variation in the saturated boiling region is predicted according to three separate correlations corresponding to different quality regions [22]: $x_e = 0 - 0.05$ associated with bubble nucleation, $x_e = 0.05 - 0.55$ corresponding mostly to bubbly/slug flow, and $x_e = 0.55 - 1.0$ consisting of predominantly annular flow and local dryout.

6.2. Comparison with HFE 7100 data

Fig. 6(a)–(d) show good agreement between predictions of the new methodology and experimental HFE 7100 pressure drop data [16] for test sections TS #1–TS #4. For each of the four sets of operating conditions shown, there is an initial decrease in pressure drop with increasing base heat flux caused by the liquid viscosity decreasing with increasing temperature. After the onset of

nucleate boiling, the pressure drop begins to increase with increasing base heat flux due to the increasing void fraction. The relation of Sato and Matsumura [35] appears to predict the base heat flux corresponding to ONB quite well. Better prediction of pressure drop trends is observed for TS #1 and TS #3, which possess higher channel aspect ratios, β , compared to TS #2 and TS #4. Uneven heating through the bottom wall and sidewalls is a possible reason for this discrepancy.

Fig. 7(a)–(d) compare predictions and experimental data for the average heat transfer coefficient for all four micro-channel test sections. The average heat transfer coefficient from the experiments is a mean of three micro-channel base locations ($z/L = 0.12, 0.50$ and 0.88). Shown is a sharp increase in the average heat transfer coefficient following the initiation of boiling. Fig. 7(a)–(d) show good agreement between the predicted and measured values.

Table 3
Micro-channel dimensions and operating conditions for comparison with water data [20].

W_{ch} μm	H_{ch} μm	W_s μm	β –	D_h μm	L cm	N –	T_{in} $^\circ\text{C}$	\dot{m} g/s	P_{out} bar	G kg/m ² s	q'' W/cm ²
231	713	236	0.32	348.9	4.48	21	60	0.9, 1.4	1.17	255, 402	22.7–199.2

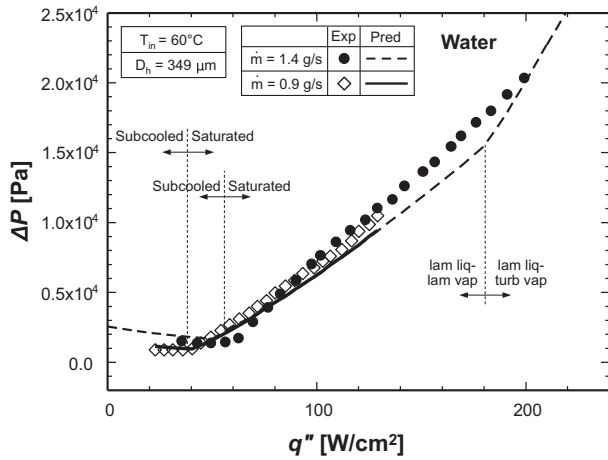


Fig. 8. Comparison of pressure drop predictions and experimental water data [20] for $\dot{m} = 1.4$ and 0.9 g/s with $T_{in} = 60^\circ\text{C}$.

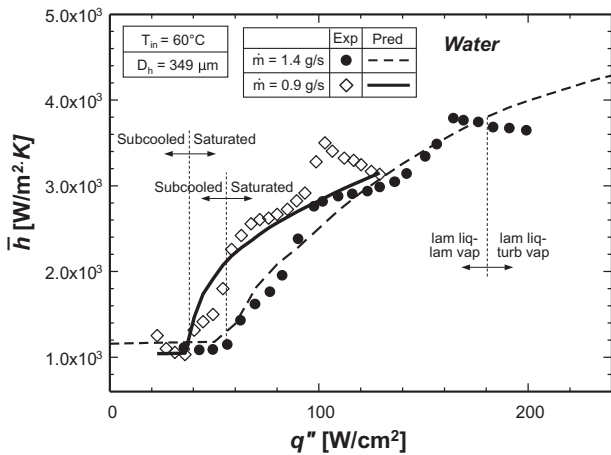


Fig. 9. Comparison average heat transfer coefficient predictions and experimental water data [20] for $\dot{m} = 1.4$ and 0.9 g/s with $T_{in} = 60^\circ\text{C}$.

6.3. Comparison with water data

Table 3 shows test section dimensions and experimental operating conditions for water data of Qu and Mudawar [20] that are used to assess the accuracy of the new predictive method. Figs. 8 and 9 compare predictions of the new predictive method for pressure drop and average heat transfer coefficient, respectively, to the data for $\dot{m} = 1.4$ and 0.9 g/s with $T_{in} = 60^\circ\text{C}$. In Fig. 8, the transition from the laminar liquid-laminar vapor to the laminar liquid-turbulent vapor ($Re_{tr} = 2000$) is predicted to occur around $q'' = 180$ W/cm², where pressure drop begins to increase rather sharply due to a large increase in void fraction. Notice that the average heat transfer coefficient from the experiments is a mean value for four micro-channel base locations ($z/L = 0.11, 0.37, 0.63$ and 0.89). Figs. 8 and 9 prove that the new predictive method is effective at reproducing the micro-channel water data of Qu and Mudawar in the range of $x_{e,out} = -0.08$ to 0.19 .

6.4. General trends of pressure drop and average heat transfer coefficient

Figs. 10 and 11 show general trends associated with the variations of pressure drop and average heat transfer coefficient, respectively, with thermodynamic equilibrium quality at the

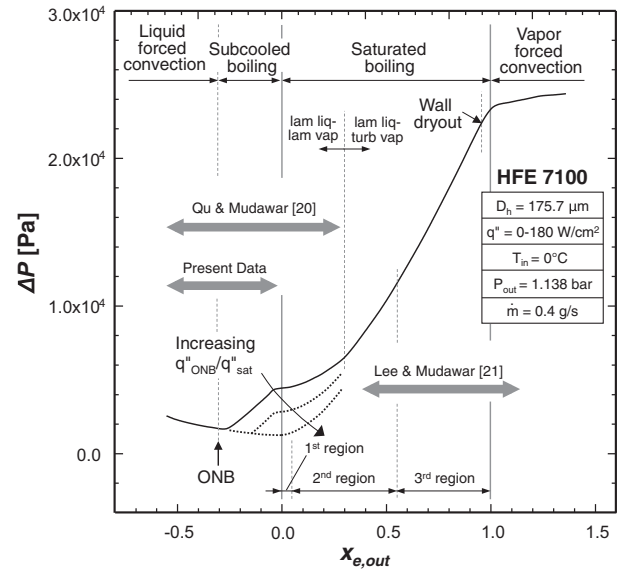


Fig. 10. Predicted pressure drop variations with thermodynamic equilibrium quality at channel outlet representing specific trends according to different heat transfer regimes.

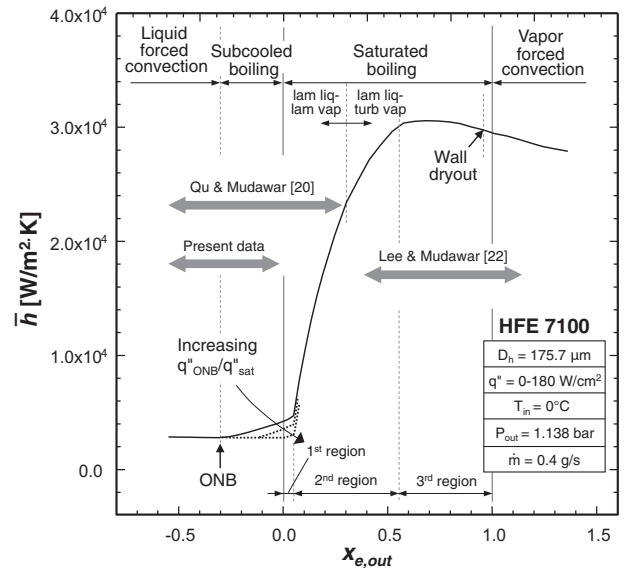


Fig. 11. Predicted average heat transfer coefficient variations with thermodynamic equilibrium quality at channel outlet representing specific trends according to different heat transfer regimes.

micro-channel outlet predicted using the new predictive methodology over a broad range of two-phase heat transfer regimes. A single micro-channel geometry of TS #1 with a base heat flux range of $0-180$ W/cm², $T_{in} = 0^\circ\text{C}$, $p_{out} = 1.138$ bar, and $G = 443$ kg/m² s is used for these predictions. The mass velocity of $G = 443$ kg/m² s examined here is chosen to produce all possible heat transfer regimes.

Fig. 10 shows an initial decrease in pressure drop with increasing $x_{e,out}$ due the aforementioned decrease in viscosity with increasing temperature. After ONB, there are slight increases in the two-phase frictional and accelerational pressure drops due to the increasing void fraction. However, a nearly constant pressure drop is predicted near $x_{e,out} = 0$, which can be explained as follows. The increasing two-phase frictional and accelerational pressure drops are counterbalanced at $x_{e,out} = 0$ by a predicted increase in expansion pressure recovery at the micro-channel outlet after

the initiation of saturated boiling. With further increases in the base heat flux, the single phase vapor regime appears in the micro-channel downstream. Fig. 5 shows local temperature and pressure variations along the micro-channel at the maximum base heat flux value of 180 W/cm².

Figs. 10 and 11 qualitatively illustrate the overall trends for pressure drop and average heat transfer coefficient, respectively, that are consistent with those observed by Qu and Mudawar [20] (subcooled and saturated boiling), Lee and Mudawar [21,22] (saturated boiling), and present data (subcooled boiling). These figures show that as q''_{ONB}/q''_{sat} decreases, ONB starts earlier, yielding a broader subcooled boiling region. This is the case for the present HFE 7100 data for TS #1 with $T_{in} = 0^{\circ}\text{C}$ and $\dot{m} = 3 \text{ g/s}$, where $q''_{ONB}/q''_{sat} = 0.18$. On the other hand, for the case of Qu and Mudawar's water data with $\dot{m} = 1.4 \text{ g/s}$ and $T_{in} = 60^{\circ}\text{C}$, $q''_{ONB}/q''_{sat} = 0.95$, hence a smaller subcooled boiling portion is observed by Qu and Mudawar data over the entire heat transfer region in Figs. 10 and 11.

7. Conclusions

This study provides a new consolidated method to predicting transport behavior of micro-channel heat sinks incurring all possible heat transfer regimes. Detailed design relations are provided to predict both pressure drop and heat transfer coefficient for different fluids and micro-channel geometries over broad ranges of operating conditions. Key findings from this study are as follows:

- (1) A new correlation is developed for subcooled flow boiling pressure drop in micro-channel heat sinks that accounts for inlet subcooling, micro-channel aspect ratio, and length-to-diameter ratio. This correlation shows excellent predictive capability, evidenced by a mean absolute error of 15.3% against subcooled HFE 7100 pressure drop data corresponding to four different micro-channel geometries.
- (2) A consolidated method for predicting pressure drop in micro-channel heat sinks is developed that is capable of tackling all possible combinations of heat transfer regimes, including single-phase liquid, subcooled boiling, saturated boiling, and single-phase vapor. The new method is shown to be highly effective at reproducing both data and trends for HFE 7100, water and R134a.
- (3) A similar consolidated method for predicting the heat transfer coefficient in micro-channel heat sinks is developed that is capable of tackling all possible combinations of heat transfer regimes. This method is also shown to reproduce both data and trends for HFE 7100, water and R134a quite effectively.

References

- [1] I. Mudawar, Assessment of high-heat-flux thermal management schemes, IEEE Trans. CPMT Components Packag. Tech. 24 (2001) 122–141.
- [2] I. Mudawar, Two-phase micro-channel heat sinks: theory, applications and limitations, ASME J. Electron. Packag. 133 (2011). 041002–2.
- [3] I. Mudawar, K.A. Estes, Optimizing and predicting CHF in spray cooling of a square surface, ASME J. Heat Transfer 118 (1996) 672–680.
- [4] L. Lin, R. Ponnappan, Heat transfer characteristics of spray cooling in a closed loop, Int. J. Heat Mass Transfer 46 (2003) 3737–3746.
- [5] J.R. Rybicki, I. Mudawar, Single-phase and two-phase cooling characteristics of upward-facing and downward-facing sprays, Int. J. Heat Mass Transfer 49 (2006) 5–16.
- [6] Y. Katto, M. Kunihiro, Study of the mechanism of burn-out in boiling system of high burn-out heat flux, Bull. JSME 16 (1973) 1357–1366.
- [7] I. Mudawar, D.C. Wadsworth, Critical heat flux from a simulated electronic chip to a confined rectangular impinging jet of dielectric liquid, Int. J. Heat Mass Transfer 34 (1991) 1465–1480.
- [8] D.C. Wadsworth, I. Mudawar, Enhancement of single-phase heat transfer and critical heat flux from an ultra-high-flux simulated microelectronic heat source to a rectangular impinging jet of dielectric liquid, ASME J. Heat Transfer 114 (1992) 764–768.
- [9] M.E. Johns, I. Mudawar, An ultra-high power two-phase jet-impingement avionic clamshell module, ASME J. Electron. Packag. 118 (1996) 264–270.
- [10] T.C. Willingham, I. Mudawar, Forced-convection boiling and critical heat flux from a linear array of discrete heat sources, Int. J. Heat Mass Transfer 35 (1992) 2879–2890.
- [11] M.B. Bowers, I. Mudawar, High flux boiling in low flow rate, low pressure drop mini-channel and micro-channel heat sinks, Int. J. Heat Mass Transfer 37 (1994) 321–332.
- [12] T.N. Tran, M.W. Wambsgans, D.M. France, Small circular – and rectangular – channel boiling with two refrigerants, Int. J. Multiphase Flow 22 (1996) 485–498.
- [13] H.J. Lee, S.Y. Lee, Heat transfer correlation for boiling flows in small rectangular horizontal channels with low aspect ratios, Int. J. Multiphase Flow 27 (2001) 2043–2062.
- [14] V. Khanikar, I. Mudawar, T. Fisher, Effects of carbon nanotube coating on flow boiling in a micro-channel, Int. J. Heat Mass Transfer 52 (2009) 3805–3817.
- [15] J. Lee, I. Mudawar, Fluid flow and heat transfer characteristics of low temperature two-phase micro-channel heat sinks – Part 1 Experimental methods and flow visualization results, Int. J. Heat Mass Transfer 51 (2008) 4315–4326.
- [16] J. Lee, I. Mudawar, Fluid flow and heat transfer characteristics of low temperature two-phase micro-channel heat sinks – Part 2. Subcooled boiling pressure drop and heat transfer, Int. J. Heat Mass Transfer 51 (2008) 4327–4341.
- [17] M.B. Bowers, I. Mudawar, Two-phase electronic cooling using mini-channel and micro-channel heat sinks: Part 2 – Flow rate and pressure drop constraints, J. Electron. Packag. 116 (1994) 298–305.
- [18] K.A. Triplett, S.M. Ghiaasiaan, S.I. Abdel-Khalik, A. LeMouel, B.N. McCord, Gas-liquid two-phase flow in microchannels Part II: Void fraction and pressure drop, Int. J. Multiphase Flow 25 (1999) 395–410.
- [19] L. Jjiang, M. Wong, Y. Zohar, Forced convection boiling in a microchannel heat sink, J. Microelectromech. Syst. 10 (2001) 80–87.
- [20] W. Qu, I. Mudawar, Flow boiling heat transfer in two-phase micro-channel heat sinks – I. Experimental investigation and assessment of correlation methods, Int. J. Heat Mass Transfer 46 (2003) 2755–2771.
- [21] J. Lee, I. Mudawar, Two-phase flow in high-heat-flux micro-channel heat sink for refrigeration cooling applications: Part I – Pressure drop characteristics, Int. J. Heat Mass Transfer 48 (2005) 928–940.
- [22] J. Lee, I. Mudawar, Two-phase flow in high-heat-flux micro-channel heat sink for refrigeration cooling applications: Part II – Heat transfer characteristics, Int. J. Heat Mass Transfer 48 (2005) 941–955.
- [23] W.L. Owens, V.E. Schrock, Local pressure gradients for subcooled boiling of water in vertical tubes, ASME Paper No. 60-WA-249, 1960.
- [24] N.V. Tarasova, A.I. Leontiev, V.I. Hlopushin, V.M. Orlov, Pressure drop of boiling subcooled water and steam-water mixture flowing in heated channels, in: Proc. 3rd International Heat Transfer Conference, Chicago, vol. 4, 1966, pp. 178–183.
- [25] E. Hahne, K. Spindler, H. Skok, A new pressure drop correlation for subcooled flow boiling of refrigerants, Int. J. Heat Mass Transfer 36 (1993) 4267–4274.
- [26] W. Tong, A.E. Bergles, M.K. Jensen, Pressure drop with highly subcooled flow boiling in small-diameter tubes, Exp. Therm. Fluid Sci. 15 (1997) 202–212.
- [27] J.G. Collier, J.R. Thome, Convective Boiling and Condensation, 3rd ed., Oxford University Press, New York, NY, 1994.
- [28] G.E. Geiger, Sudden contraction losses in single and two-phase flow, Ph.D. Thesis, University of Pittsburgh, PA, 1964.
- [29] J. Schmidt, L. Friedel, Two-phase pressure drop across sudden contractions in duct areas, Int. J. Multiphase Flow 23 (1997) 283–299.
- [30] F.F. Abdelall, G. Hahn, S.M. Ghiaasiaan, S.I. Abdel-Khalik, S.S. Jeter, M. Yoda, D.L. Sadowski, Pressure drop caused by abrupt flow area changes in small channels, Exp. Therm. Fluid Sci. 29 (2005) 425–434.
- [31] S.W. Churchill, R. Usagi, A general expression for the correlation of rates of transfer and other phenomena, AIChE J. 18 (1972) 1121–1128.
- [32] D. Copeland, Manifold microchannel heat sinks: analysis and optimization, ASME/JSME Thermal Eng. 4 (1995) 169–174.
- [33] R.K. Shah, A.L. London, Laminar Flow Forced Convection in Ducts: A Source Book for Compact Heat Exchanger Analytical Data, Academic press, New York, NY, 1978 (Supl 1).
- [34] W. Zhi-qing, Study on correction coefficients of laminar and turbulent entrance region effect in round pipe, Appl. Math. Mech. 3 (1982) 433–446.
- [35] T. Sato, H. Matsumura, On the conditions of incipient subcooled boiling and forced-convection, Bull. JSME 7 (1963) 392–398.
- [36] S.M. Zivi, Estimation of steady-state steam void-fraction by means of the principle of minimum entropy production, ASME J. Heat Transfer 86 (1964) 247–252.
- [37] F.P. Incropera, D.P. Dewitt, Fundamentals of Heat and Mass Transfer, 5th ed., Wiley, New York, NY, 2002.
- [38] M. Al-Arabi, Turbulent heat transfer in the entrance region of a tube, Heat Transfer Eng. 3 (1982) 76–83.
- [39] S.M. Kim, I. Mudawar, Analytical heat diffusion models for different micro-channel heat sink cross-sectional geometries, Int. J. Heat Mass Transfer 53 (2010) 4002–4016.
- [40] S.M. Kim, I. Mudawar, Analytical heat diffusion models for heat sinks with circular micro-channels, Int. J. Heat Mass Transfer 53 (2010) 4552–4566.